

## Chapter 3

# Life and Death of Dissipative Structures

In this transition chapter we focus on the emergence of convection and how patterns that have developed further desegregate. This rather intuitive example helps us to introduce a few general ideas and techniques to analyse instabilities (§3.1). The theory that allows us to interpret their disorganisation, presented here from a purely phenomenological perspective (§3.2) will be re-examined in Chapters 4 and 6.

### 3.1 Emergence of Dissipative Structures

#### 3.1.1 *Qualitative analysis of the instability mechanism*

Let us go back in more detail on the argument previously sketched in relation with Figure 1.3, p. 11, to explain the onset of convection. The two parts of the mechanism, instability due to differential buoyancy and stability through dissipation (viscous relaxation and heat diffusion) will first be qualitatively analysed in terms of *characteristic times*.

Let us consider a horizontal layer (height  $h$ ) of fluid heated from below (Figure 3.1):

$$T_b = T_t + \Delta T > T_t$$

(‘b’ for ‘bottom’ and ‘t’ for ‘top’). The fluid is initially at rest in a regime of *pure conduction*. The temperature profile is linear

$$T_0(z) = T_b - \beta z \quad \text{with} \quad \beta = \Delta T/h,$$

and notations imply that the temperature gradient  $\beta$  is positive in case of heating from below.

The corresponding density distribution is given by the equation of state which, in a first approximation, reads:

$$\rho(T) = \rho_{\text{ref}} (1 - \alpha (T - T_{\text{ref}})) \quad (3.1)$$

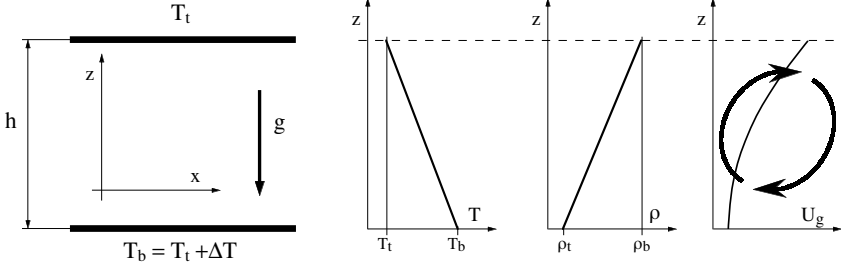


Fig. 3.1 Left: Geometry of the convection experiment. Right: Profiles of temperature  $T(z)$ , density  $\rho(z)$  and gravitational potential energy  $U_g(z)$  for a fluid particle at altitude  $z$ , indicating the tendency to restore a stable density stratification with heavy fluid at the bottom.

where  $T_{\text{ref}}$  is a reference temperature,  $\rho_{\text{ref}} = \rho(T_{\text{ref}})$ , and  $\alpha$  is the thermal expansion coefficient ( $1/273$  for an ideal gas), hence  $\rho_0(z) = \rho(T_0(z))$ .

A first characteristic time, a transport time  $\tau_b$ , can be defined from the buoyancy (hence subscript ‘b’). Assume a fluid particle experiencing a temperature fluctuation  $\theta$  at some height  $z$ , i.e.  $T(z) = T_0(z) + \theta$ , from (3.1) the differential force to which it is submitted is  $\rho g \alpha \theta$ . The quantity  $g \alpha \theta$  is thus an acceleration, homogeneous to a length divided by the square of a time. Natural length and temperature scales are  $h$  and  $\Delta T$ , respectively. We can thus define the time  $\tau_b$  through:

$$\frac{h}{\tau_b^2} = g \frac{\Delta \rho}{\rho} \sim g \alpha \Delta T.$$

Physically,  $\tau_b$  is the typical time a hot (cold) bubble would take to move up (down) over a distance  $h$  with a constant acceleration due to thermal expansion.

Dissipative processes, viscous friction (Stokes law, kinematic viscosity  $\nu = \mu/\rho$ ) and thermal conduction (Fourier law, thermal diffusivity  $\kappa = \chi/C$  where  $\chi$  is the thermal conductivity and  $C$  the specific heat) are diffusive in essence. The relaxation times associated with these processes can be deduced from the form of a diffusion equation,  $\partial_t q \propto \nabla^2 q$ , in which the proportionality coefficient is the diffusivity, homogeneous to  $[\ell]^2 [t]^{-1}$ , hence here:

$$\nu = h^2 / \tau_\nu, \quad \kappa = h^2 / \tau_\theta.$$

(See also Exercise 1.5.1.)

The result of the competition between the destabilising mechanism and the stabilising processes can be estimated by forming the ratio:

$$R = \frac{\tau_v \tau_\theta}{\tau_c^2} = \frac{\alpha g \Delta T h^3}{\kappa \nu} \quad (3.2)$$

called the *Rayleigh number*. By construction, it is a dimensionless number. Convection develops when the buoyancy is more effective ( $\tau_b$  short) than the dissipative processes ( $\tau_v$  and  $\tau_\theta$  long) and thus when  $R$  is large. This strictly dimensional analysis is qualitative and cannot help us to determine the value of  $\Delta T$  necessary to induce convection. It is the reason why we go one step further and develop a more quantitative model of the instability. The detailed analysis is the subject of Exercise 3.3.2.

### 3.1.2 Simplified model

In order to study the stability of the base flow, here the fluid at rest ( $\mathbf{v}_0 \equiv 0$ ) in a regime of pure conduction with linear temperature profile ( $T_0(z) \sim -\beta z$ ,  $\beta = \Delta T/h$ ), we must derive the equations governing small perturbations around this state, a temperature fluctuation  $\theta$  defined by  $T = T_0(z) + \theta$  and a velocity fluctuation  $\mathbf{v}$ . We thus insert the full solution into the primitive equations (here: continuity + Navier–Stokes + Fourier in a fluid), expand these equations in powers of the perturbations, and finally keep only the first order terms (linear stability theory).

The analysis of the mechanism (Chapter 1, §1.3.1) points out a direct coupling of the horizontal modulations of the temperature fluctuation and the vertical velocity component. Accordingly, we assume that a model involving just  $\theta$  and  $v_z$ , depending only on the horizontal coordinate  $x$  and time  $t$ , will capture the physics.

- *Equation for the vertical velocity:* The unperturbed temperature field  $T_0(z)$  induces a density distribution  $\rho_0(z) = \rho(T_0(z))$  through (3.1). The differential buoyancy generated by a temperature fluctuation  $\theta$  reads:

$$-g(\rho - \rho_0) = -g[\rho(T_0 + \theta) - \rho(T_0)] \approx \rho_0 \alpha g \theta,$$

where the minus sign comes from the fact that the vertical unit vector is oriented up while the force is directed down. It appears as an external force term in the  $z$  component of the Navier–Stokes equation:

$$\partial_t v_z = \nu \partial_{x^2} v_z + \alpha g \theta, \quad (3.3)$$

where the first term on the r.h.s. corresponds to viscous diffusion (only along  $x$ ). The term  $\mathbf{v} \cdot \nabla \mathbf{v}$  is of higher order since there is no velocity at

order zero. Also, one can notice that  $\theta > 0$  implies  $\partial_t v_z > 0$ , i.e. an upward acceleration as guessed intuitively.

- *Heat equation:* The Fourier equation must be written for a fluid particle (cf. p. 7) since, as already mentioned, it is its advection in a spatially varying temperature field that plays the essential role in the feedback loop, hence:

$$\frac{d}{dt}T = \partial_t T + \mathbf{v} \cdot \nabla T = \kappa \partial_{x^2} T.$$

Expanding the term  $\mathbf{v} \cdot \nabla T$  to first order (linearisation) we find:

$$v_z \partial_z [T_0(z) + \theta] = v_z \partial_z T_0(z) = -v_z \beta,$$

which comes from the temperature field at order zero (the second-order term  $v_z \partial_z \theta$  is neglected). This leads to:

$$\partial_t \theta = \kappa \partial_{x^2} \theta + \beta v_z. \quad (3.4)$$

*Remark:* Lateral boundary conditions have not yet been specified. Here, we tacitly assume that we deal with a horizontally unbounded layer, or at least that the horizontal dimensions are large when compared to the sole characteristic length in the problem, the height  $h$  of the layer. Moreover, the horizontal velocity component and the pressure are absent from the problem at this stage. They are only indirectly coupled to  $v_z$  and  $\theta$  by the need to ensure the continuity of the fluid and the closing of flow lines. The model is thus highly simplified. This deficiency will impede us to determine the critical wavelength that will thus be fixed from the outside by dimensional considerations. Anyway, we shall now illustrate the extension to continuous media of the stability analysis introduced at the beginning of the previous chapter using the simplified model (3.3, 3.4).

### 3.1.3 Normal mode analysis, general perspective

The system formed by (3.3, 3.4) is typical of linear stability problems in continuous media, i.e. a system of linear partial differential equations (with constant coefficients in the simplest case). It presents itself as an *initial value problem* for the perturbations that we write formally as:

$$\partial_t \mathbf{V} = \mathcal{L}_r(\partial_x, \dots) \mathbf{V}, \quad (3.5)$$

where  $\mathbf{V}$  represents the set of perturbations. The linear operator  $\mathcal{L}_r$  contains spatial partial derivatives  $(\partial_x, \dots)$  and also depends on a set of *control parameters* denoted as  $r$ . In general, the instability can be controlled using

a single quantity that can be varied from the outside (for convection, it is simply the applied temperature gradient  $\beta$ ), all other parameters of the system being kept fixed.

Problem (3.5) is linear. Its solution can therefore be searched by means of a *superposition*:

$$\mathbf{V}(\mathbf{x}, t) = \sum_n A_n \mathbf{X}_n(\mathbf{x}, t), \quad (3.6)$$

to be introduced in the differential problem. Setting:

$$\mathbf{X}(\mathbf{x}, t) = \exp(st) \hat{\mathbf{X}}(\mathbf{x}), \quad (3.7)$$

and inserting this assumption in (3.5), we get

$$s \hat{\mathbf{X}}(\mathbf{x}) = \mathcal{L}_r \hat{\mathbf{X}}(\mathbf{x}). \quad (3.8)$$

The stability study then comes to an *eigenvalue problem*. The states  $\hat{\mathbf{X}}(\mathbf{x})$  are called the *normal modes* of the problem. These modes have spatial structures that mathematically express the physical *coherence* of the processes at work in the system. On general grounds, the eigenvalues  $s$  are complex since the spectrum is entirely real only when the operator can be made self-adjoint for some well-chosen scalar product (see §A.3).

The nature of the spectrum of  $\mathcal{L}_r$  depends on the applied *confinement* conditions (Exercise 3.3.1). When the system is unbounded in some directions of space, the spectrum is formed with continuous branches, indexed by as many continuous parameters as there are unbounded directions. For example if the mechanism singles out a specific direction ('vertical' in the case of convection), and if the system is invariant under translations in two complementary directions ('horizontal'), performing a Fourier transform, one looks for normal modes in the form:

$$\hat{\mathbf{X}}_n(x, y, z) = \exp(i(k_x x + k_y y)) \tilde{\mathbf{X}}_n(z), \quad (3.9)$$

which defines the *wavevector*  $\mathbf{k}_\perp = (k_x, k_y)$  as an indexing parameter. Under the substitution  $\nabla_\perp \equiv (\partial_x, \partial_y) \mapsto i\mathbf{k}_\perp$ , the operator  $\mathcal{L}_r = \mathcal{L}_r(\partial_x, \dots)$  is transformed into an ordinary differential operator in  $z$ , the only remaining independent variable, i.e.  $\mathcal{L}_r(ik_x, ik_y, d/dz)$ . The wavevector  $\mathbf{k}_\perp$  thus labels the eigenmode branches in addition to a discrete index related to the confinement direction  $z$ . Equation (3.8) has nontrivial solutions provided that the growth rate and the wavevector  $\mathbf{k}_\perp$ , introduced in (3.7) and (3.9) fulfil a compatibility condition called the *dispersion relation*:

$$s = s_n(r, \mathbf{k}_\perp). \quad (3.10)$$

Let us examine a few questions relative to confinement effects.

- As for convection between unbounded horizontal plates, when the system is rotationally invariant in the plane orthogonal to the direction in which the mechanism is operating, then  $s_n$  can only depend on  $k = |\mathbf{k}_\perp|$  and not on its orientation.
- When the system is bounded in two space directions, e.g.  $y$  and  $z$ , and translationally invariant in the last one  $x$ , the continuous component  $k_y$  is replaced by a discrete index.
- When the system is bounded in all three directions, i.e. when its size is of the order of the scale over which the instability mechanism is operating in all directions, the spectrum loses its last continuous dependence on  $k$  and becomes fully discrete. The eigenvalues are all distinct, except for degeneracy linked to physical symmetries. The spatial structure of the normal modes is specific to the geometry considered and mirrors spatial resonance properties of the mechanism with the shape of the set-up. The situation is then the closest to the one considered in the previous chapter, but with infinite series of eigenvalues and normal modes to acknowledge the fact that we deal with continuous media with infinitely many degrees of freedom.

Considering the case of a system unbounded in just one direction (single continuous parameter  $k$ ), we can write

$$s_n(k, r) = \sigma_n(k, r) - i\omega_n(k, r).$$

Given  $r$  and  $k$ , the modes can then be ordered by decreasing values of their real part  $\sigma_n(k, r)$ , which, from definition (3.7), allows the distinction between *stable* normal modes with  $\sigma_n < 0$  (damped) and *unstable* modes with  $\sigma_n > 0$  (amplified). The dissipative character of the medium implies that modes with the shortest wavelengths are strongly damped, i.e.  $\sigma_n(k) \rightarrow -\infty$  when  $k \rightarrow \infty$ .

A given mode  $n$  with wavevector  $k$  bifurcates when on its way from stable to unstable it becomes *neutral*, upon variation of the control parameter. The corresponding *marginal* condition, superscript '(m)', is defined thus by the condition  $\sigma_n(k, r) = 0$ . Once solved for  $r$ , this condition reads:

$$r = r_n^{(m)}(k)$$

Let us assume that, as in convection, increasing the stress corresponds to increasing the control parameter  $r$ , the marginal curve for some mode  $n$  usually reaches its minimum for some  $k = k_n^{(c)}$  called the *critical wavevector* for that mode. The quantity  $r_n^{(m)}(k_n^{(c)}) = r_n^{(c)}$  is the corresponding *threshold*.

Now, according to the general discussion about stability in the previous chapter, *linear instability* takes place as soon as one normal mode becomes unstable. The linear instability threshold  $r_c$  is therefore the minimum over  $n$  of all the so-defined  $r_n^{(c)}$ , achieved for some  $n = n_c$ . The wavevector corresponding to that mode is called the critical wavevector of the instability. The latter is hence characterised by the set  $n_c, r_c = r_{n_c}^{(c)}, k_c = k_{n_c}^{(c)}$ .

Apart from its growth properties, the rest of the time dependence of a mode depends on the value of  $\omega_n(k, r)$ . When  $\omega_n = 0$ , the mode is said to be *stationary*, whereas when  $\omega_n \neq 0$ , one speaks of an *oscillatory* mode. The value of the angular frequency at threshold,  $\omega_c = \omega_{n_c}(k_c, r_c)$ , thus allows one to distinguish stationary from oscillatory instabilities. The classification of instabilities according to the spatiotemporal structure of their critical mode will be re-examined in §3.1.6.

### 3.1.4 Back to the model

Let us come back to the simplified model (3.3, 3.4). We assume that the fluid layer is unbounded in the  $x$  direction so that, according to (3.7–3.9), solutions are searched in the form  $\{v_z, \theta\} = \{V, \Theta\} \exp(st) \exp(ikx)$ . We obtain:

$$\begin{aligned} sV &= -\nu k^2 V + \alpha g \Theta, \\ s\Theta &= -\kappa k^2 \Theta + \beta V, \end{aligned}$$

which is in fact a homogeneous algebraic system of two equations for two unknowns:

$$\begin{aligned} (s + \nu k^2)V - \alpha g \Theta &= 0, \\ -\beta V + (s + \kappa k^2)\Theta &= 0. \end{aligned}$$

The system has non-trivial solutions only if its determinant cancels:

$$(s + \nu k^2)(s + \kappa k^2) - \alpha g \beta = s^2 + (\nu k^2 + \kappa k^2)s + \kappa \nu k^4 - \alpha g \beta = 0. \quad (3.11)$$

This *compatibility condition* linking the growth-rate  $s$  to the wavevector  $k$  of the perturbation is here the expression taken by the dispersion relation (3.10). We get a single branch (and thus no discrete index) since the differential problem in  $z$  has been replaced by an algebraic system, due to our neglect of the  $z$ -dependence of the fluctuations.

If the real part of  $s(k)$  is negative, the mode is damped and the layer is *stable* against a perturbation with wavelength  $\lambda = 2\pi/k$ . Otherwise the fluctuation is amplified and the mode  $k$  is *unstable*.

Let us estimate the threshold from (3.11). Here it is a quadratic equation in  $s$  that can have two real or complex roots.<sup>1</sup> The discriminant

$$\Delta = (\nu k^2 + \kappa k^2)^2 + 4[\alpha g \beta - (\nu k^2)(\kappa k^2)] = (\nu k^2 - \kappa k^2)^2 + 4\alpha g \beta$$

can be negative, and the corresponding solutions to (3.11) have non-zero imaginary parts, only when  $\beta$  is sufficiently large and negative, in the case of strong heating from above. But in this case the modes are always damped since the sum of the roots

$$S = -\frac{1}{2}(\nu k^2 + \kappa k^2) \quad (3.12)$$

is then negative. This analysis thus confirms the intuition according to which heating must be from below in order to have an instability. Moreover, if there is an instability, it can only be *stationary*, with two real roots, one positive, the other negative since their sum is negative. In order to determine the sign of the roots we have just to consider their product

$$P = (\nu k^2)(\kappa k^2) - \alpha g \beta. \quad (3.13)$$

The change of sign takes place at  $\beta = \beta^{(m)}(k)$  with

$$\beta^{(m)}(k) = \frac{\nu \kappa k^4}{\alpha g}. \quad (3.14)$$

As long as  $\beta < \beta^{(m)}$ , the product is positive and the two roots negative, mode  $k$  is stable. When  $\beta > \beta^{(m)}$ , it becomes negative and one of the roots is positive, the mode is unstable, convection sets in. The value  $\beta = \beta^{(m)}(k)$  of the applied temperature gradient thus defines the *marginal stability condition* that makes mode  $k$  neutral. One can observe that the negativity of the sum and the positivity of the product, the two stability factors, come from stabilising dissipative processes and that the instability factor involves a term in  $\beta$  arising from the advection of the fluctuation through the layer submitted to the temperature gradient.

The marginal stability condition (3.14) implies an increase of the marginal temperature gradient as  $k^4$  for  $k$  large, which expresses the growing efficiency of the stabilising mechanisms as the scale of the fluctuations decreases (Figure 3.2, left). According to this relation, the longer the wavelength, the lower the threshold. However one should not conclude that the fluid layer is unstable at  $k = 0$  for  $\beta = 0$ , i.e.  $\Delta T = 0$ . because this low- $k$  behaviour is an artefact of the one-dimensional character of the model that

<sup>1</sup>Let  $s_{1,2}$  be the two roots, one has  $0 = (s - s_1)(s - s_2) = s^2 - (s_1 + s_2)s + s_1 s_2 = s^2 - Ss + P$  where  $S$  is the sum of the roots and  $P$  their product. The discriminant is  $\Delta = S^2 - 4P$  and the roots are  $s_{1,2} = s_{\pm} = \frac{1}{2}(S \pm \sqrt{\Delta})$ .

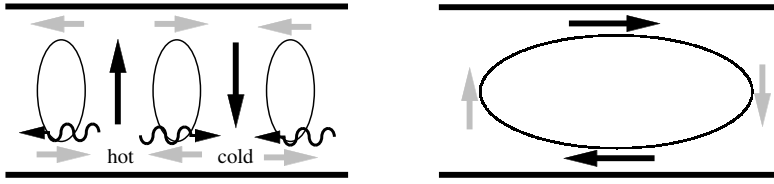


Fig. 3.2 Left: For  $\lambda = 2\pi/k \ll h$ , viscous dissipation associated with the horizontal shear  $\partial_x v_z$  (black arrows) and thermal diffusion (undulated arrows) combine their effects to prevent convection, while the vertical shear  $\partial_z v_x$  (grey arrows) can be neglected. Right: When  $\lambda \gg h$  the horizontal shear (grey arrows) becomes negligible while the vertical shear (black arrows) becomes dominant.

neglects the  $z$ -dependence of the fluctuations and the associated dissipation processes: The viscous damping by the horizontal component of the flow that closes the streamlines can no longer be neglected as  $k \rightarrow 0$  (Figure 3.2, right), hence the need for a corrected argument valid at small  $k$ .

Keeping  $v_z$  as a reference since it is directly involved in the instability mechanism, one can estimate the order of magnitude of  $v_x$  from the continuity equation

$$\partial_x v_x + \partial_z v_z = 0.$$

Boundary conditions on  $v_z$  are at the horizontal plates, a distance  $h$  apart, and imply a  $z$ -dependence such that  $\partial_z v_z \sim v_z/h$  and therefore  $kv_x \sim v_z/h$  or  $v_x \sim v_z/kh$ . But the presence of  $v_x$  imposes us to take the  $x$ -component of the Navier–Stokes equation into account. We can simplify it as:

$$-kp/\rho - \nu v_x/h^2 \simeq 0,$$

and introduce the so-evaluated pressure in the equation for  $v_z$ , which yields:

$$\partial_t v_z = -\partial_z p/\rho + \nu(\partial_{x^2} + \partial_{z^2})v_z + \alpha g\theta. \quad (3.15)$$

A sketchy analysis of the space dependence of the different perturbations then shows that, once expressed in terms of  $v_z$  using the continuity equation,  $\partial_z p/\rho$  goes as  $\nu v_z/k^2 h^4$ , so that the pressure term dominates those involving  $v_z$  on the r.h.s. of (3.15). As a matter of fact, it diverges as  $k^{-2}$  when  $k \rightarrow 0$ , while the second term tends to zero as  $k^2$  and the third one does not vary with  $k$ . We thus arrive at an effective equation for  $v_z$  replacing (3.3):

$$\partial_t v_z = -\nu(1/h^4 k^2)v_z + \alpha g\theta,$$

only valid in the limit  $k \ll 1/h$  (the minus sign expresses the fact that it is indeed a damping term). In this limit, it suffices to replace  $-k^2$  by  $-1/h^2$

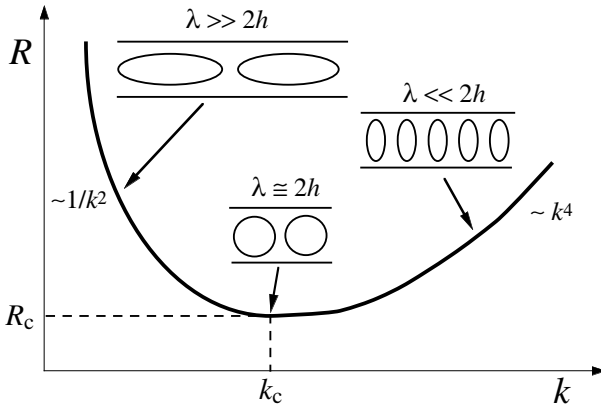


Fig. 3.3 Marginal stability curve from the semi-quantitative argument.

in the heat equation (3.4) to account for the dominant dissipative process. A stability analysis parallel to that leading to (3.14) yields:

$$\kappa\nu/(h^6 k^2) - \alpha g\beta^{(m)} = 0,$$

so that the marginal stability condition for small wavevectors reads:

$$\beta^{(m)}(k) = \frac{\nu\kappa}{\alpha gh^6 k^2} \tag{3.16}$$

thus showing a divergence as  $1/k^2$  for  $k \rightarrow 0$  that can be demonstrated through a detailed calculation (Exercise 3.3.2, see Figure 3.16, p. 118).

Between the divergence as  $k^4$  for  $k \gg 1/h$  and as  $1/k^2$  for  $k \ll 1/h$ , we must find a minimum corresponding to some optimum between the stabilising effects of different origins and the destabilising buoyancy force. This optimum is achieved for some intermediate value of the wavevector that, for dimensional reasons, can only be related to the thickness of the layer (Figure 3.3). Assuming that the diameter of the convection cells is, at threshold, of the order of  $h$ , i.e.

$$k_c = \frac{2\pi}{\lambda_c} = \frac{\pi}{h},$$

and inserting this value of the *critical wavevector* in the expression of  $\beta_m$  we get the *instability threshold* beyond which the convection regime develops, in the form of regular structures with typical wavelength  $\lambda_c = 2\pi/k_c \simeq 2h$ . Using expression (3.2) for the Rayleigh number, (3.14) yields:

$$R_c \sim \pi^4.$$

The semi-quantitative argument developed so far stresses on the physics of the processes at stake. The threshold value turns out to be grossly underestimated because a large part of the dissipating processes is badly evaluated, but it remains reasonable as an order of magnitude. We should notice that the model, however simple it may be, reproduces the two main characteristics of the instability: its stationary character and the general shape of the marginal stability curve with a correct asymptotic behaviour for  $k \ll k_c$  and  $k \gg k_c$ . Similar simplified analyses will be developed as exercises to study the effects of molecular diffusion on convection in binary mixtures (Exercise 3.3.3), the stability of an angular momentum stratification in a cylindrical shear experiment (Taylor–Couette instability, Exercise 3.3.5), or the emergence of spatial structures in reaction–diffusion systems (Turing instability, Exercise 3.3.4).

### 3.1.5 Vicinity of the threshold: linear stage

Studying the linear dynamics of fluctuations in the neighbourhood of the threshold is best developed by first turning equations (3.3, 3.4) into dimensionless form. In order to do this, we have to choose length, time, and temperature scales. The thickness  $h$  of the layer is the obvious natural length scale. The thermal diffusion time over distance  $h$ ,  $\tau_\theta = h^2/\kappa$ , being chosen as the time scale (the alternate possibility would be the viscous time  $\tau_v = h^2/\nu$ ), the velocity scale then reads  $h/\tau_\theta = \kappa/h$ . Since it is preferable to keep  $\Delta T$  as the control parameter, the composite quantity<sup>2</sup>  $\kappa\nu/\alpha gh^3$  is taken as the temperature scale. Performing the changes  $x \mapsto hx$ ,  $t \mapsto \tau_\theta t, \dots$  in (3.3, 3.4) we obtain

$$\partial_t v_z = P (\partial_{xx} v_z + \theta), \quad (3.17)$$

$$\partial_t \theta = \partial_{xx} \theta + R v_z. \quad (3.18)$$

A second dimensionless number has been introduced:

$$P = \frac{\nu}{\kappa} = \frac{\ell^2/\kappa}{\ell^2/\nu} = \frac{\tau_\theta}{\tau_v}. \quad (3.19)$$

Called the *Prandtl number*, it characterises the physical properties of the fluid, specifying which of the viscous diffusion ( $\tau_v = h^2/\nu$ ) or the thermal diffusion ( $\tau_\theta$  defined above) is the dominant relaxation process.

In gases  $P$  is of the order of unity and varies little with the nature of the gas since momentum ( $\tau_v$ ) is transported by the molecules themselves at

<sup>2</sup>From expression (3.2) for the Rayleigh number, it is easily checked that it is homogeneous to a temperature.

the same rate as energy ( $\tau_\theta$ ). In condensed fluids this number can largely vary. For example, in liquid metals (e.g. mercury) it is very small, typically  $< 10^{-2}$ , since energy is efficiently transported by conduction electrons while atoms must be moved to smooth out velocity fluctuations, hence  $\tau_\theta \ll \tau_v$ . In insulating fluids, thermal diffusion mainly involves molecular vibrations that keep the same order of magnitude whatever the fluid, while the viscosity can vary by large amounts.  $P$  is of the order of 2–10 in water or alcohol,  $10^2$ – $10^4$  in silicon oils depending on the polymerisation degree (molecular weight), and essentially infinite for the Earth mantle which is extraordinarily viscous and in which convection develops on geological times only.

In the limit  $P \gg 1$ , the flow adjusts itself to the temperature field instantaneously, which can be understood from the consideration of equation (3.17) written as

$$P^{-1} \partial_t v_z \simeq 0 = \partial_{xx} v_z + \theta,$$

showing that  $v_z$  is merely obtained by integrating  $\theta$  over space. The dynamics is therefore simplified since we have just one relevant scalar field. On the contrary, when  $P$  is small, the inertia of the fluid cannot be neglected and a full hydrodynamic problem is recovered, with the vector nature of the velocity field and the incompressibility condition playing a crucial role.

Let us stay in the limit  $P \gg 1$  and consider the critical mode  $(v_z, \theta) \sim \sin(k_c x)$  with  $k_c \simeq \pi$  ( $\pi/h$  if the physical dimension is restored). Within the framework of the simplified model we get:

$$v_z = \theta / \pi^2,$$

and upon insertion in (3.18):

$$\partial_t \theta = -\pi^2 \theta + R v_z = (-\pi^2 + R/\pi^2) \theta.$$

Dividing both members of this equation by  $\pi^2$  and defining:

$$\tau_0 = \frac{1}{\pi^2} \quad \text{and} \quad r = \frac{R - R_c}{R_c}, \quad (3.20)$$

with here  $R_c = \pi^4$  (but this value is only anecdotal) we simply get:

$$\tau_0 \partial_t \theta = r \theta. \quad (3.21)$$

The coefficient  $\tau_0$  therefore presents itself as a characteristic evolution time ( $\tau_\theta/\pi^2$  in physical units) for convection, while  $r$  measures the relative distance to the threshold and is, of course, our control parameter.

Defining  $A$  as the amplitude of the most unstable convection mode and setting:

$$\theta \propto A(t) \sin(k_c x), \quad (3.22)$$

we get from (3.21) the linear evolution equation for  $A$

$$\frac{d}{dt}A = \sigma A, \quad (3.23)$$

where  $\sigma = r/\tau_0$  is its effective growth rate, which substantiates (1.16) introduced on phenomenological grounds in Chapter 1, p. 12. The corresponding time  $\tau = 1/\sigma = \tau_0/r$  therefore diverges as  $r^{-1}$  close to the threshold ( $r \ll 1$ ), a phenomenon called the *critical slowing-down*. Amplitude  $A$  plays the role of an *effective degree of freedom* for the fluid layer as a whole.

Result (3.23) is valid much more generally than suggested by the derivation above on the special case  $P \rightarrow \infty$ , and indeed holds in the vicinity of any linear instability. This is a consequence of the fact that  $\sigma$  is a non-singular function of the parameters, and thus can be expanded in Taylor series. Since the condition that defines the threshold  $r_c = 0$  is precisely  $\sigma = 0$ , generically the expansion begins with its first order term  $\sigma = r \partial_r \sigma|_c$ , hence the observed behaviour of  $\sigma$  as a function of  $r$ .

The argument just produced can be repeated for a value of  $k$  different from the critical value  $k_c$  provided that we replace the threshold  $R_c$  by the corresponding marginal value  $R^{(m)}(k)$ . As long as  $k$  stays sufficiently close to  $k_c$ , the natural characteristic evolution time has no reason to be very different from  $\tau_0$ , so that we can write at lowest order

$$\tau_0 \sigma(k) = \frac{R - R^{(m)}(k)}{R^{(m)}(k)}. \quad (3.24)$$

On the other hand, any curve in the vicinity of an *extremum* is generically equivalent to a parabola. The marginal curve close to its minimum at  $(k_c, R_c)$  is not an exception so that, for  $k = k_c + \delta k$  and  $\delta k/k_c \ll 1$ , we can write

$$\frac{R^{(m)}(k) - R_c}{R_c} = \xi_0^2 \delta k^2, \quad (3.25)$$

where  $\xi_0^2$  presents itself as the square of a characteristic length, the *coherence length*, which accounts for the curvature of the marginal stability curve at threshold.

### 3.1.6 Classification of unstable modes

One can arrange (3.24) and (3.25) together to write down the real part of the dispersion relation in the condensed form:

$$\tau_0 \sigma(k) \simeq r - \xi_0^2 (k - k_c)^2. \quad (3.26)$$

When the minimum of the marginal stability curve is reached for  $k_c \neq 0$ , case considered up to now of convection in a simple fluid, one says that the instability is *cellular*. Otherwise, it may happen that the most unstable mode is for  $k_c = 0$  and the instability is then termed *homogeneous*. This situation, which occurs for example when convection takes place between horizontal plates that are bad thermal conductors, is often difficult to treat since the system is sensitive to lateral boundary conditions and/or any kind of slowly varying perturbations, while when  $k_c \neq 0$ , each cell with width  $\lambda_c/2$  plays its own game, without worrying about lateral boundaries as soon as they are sufficiently far apart, say three or four wavelengths.

From a temporal viewpoint, Rayleigh–Bénard convection in a simple fluid is a *stationary* instability and the imaginary part  $\omega(k)$  of the dispersion relation is identically zero. In other cases, the instability may be *oscillatory* with  $\omega_c \neq 0$ , where  $\omega_c$  is the angular frequency at threshold. When the instability sets in with  $k_c \neq 0$  and  $\omega_c \neq 0$ , the critical mode is in fact a *wave* propagating at some *phase velocity*  $c$  since, factoring out  $k_c$  one can write  $\exp(i(k_c x - \omega_c t)) \equiv \exp(ik_c(x - ct))$ , as will be done in Chapter 7.

The real part  $\sigma$  of the eigenvalue of the marginal mode is well approximated by (3.26) in the neighbourhood of the threshold  $(r_c, k_c)$ . In the same way, its imaginary part  $\omega(k)$  can be expanded as:

$$\omega(k) = \omega_c + r \partial_r \omega|_c + \delta k \partial_k \omega|_c + \frac{1}{2} \delta k^2 \partial_{kk} \omega|_c, \quad (3.27)$$

where derivatives with respect to  $r$  or  $k$  are computed at threshold.

The coefficient of  $\delta k$  (third term on the r.h.s.) corresponds to the *group velocity* of the waves. This can be seen by looking at a wave packet formed by superposition of elementary waves written as  $V(x, t) = \int A(k) \exp i(kx - \omega t) dk$ , where  $A(k)$  is the amplitude of mode  $k$  presenting a peak at some wavevector  $k = k_0$ . Setting  $\omega_0 = \omega(k_0)$ , we get:

$$V(x, t) = \exp i(k_0 x - \omega_0 t) \int A(k_0 + \delta k) \exp[i \delta k(x - \partial_k \omega|_{k_0} t) + \mathcal{O}(\delta k^2)] d\delta k.$$

In the long time limit ( $t \gg 1/\omega_0$ ),  $V$  is negligible everywhere except where the argument of the exponential is zero (‘stationary phase’ approximation) since elsewhere the rapid oscillations of the complex exponential “kill” the signal. This happens when  $x/t = \partial_k \omega|_{k_0}$  which shows that this quantity is precisely the velocity of the wavepacket. In the same way, the coefficient of  $\delta k^2$  in (3.27) accounts for the *dispersion* of the wavepacket, i.e. its smearing out due to changes in phase velocity. In a non-dispersive medium, the phase velocity is independent of the wavevector, i.e.  $\partial_k(\omega/k) = 0$ , so that  $c_g \equiv \partial_k \omega = \omega/k \equiv c$  and of course  $\partial_{kk} \omega \equiv 0$ .

The Taylor–Couette instability of a fluid sheared between two coaxial cylinders rotating at different angular speeds (Exercise 3.3.5) is also cellular and stationary. In chemistry, the Belousov–Zhabotinsky reaction is an example of homogeneous oscillatory instability. Finally, in some circumstances, convection in binary fluid mixture develops in the form of dissipative waves (Exercise 3.3.3).

## 3.2 Disintegration of Dissipative Structures

The study of the transition to turbulence of structures generated by an instability mechanism consists of several steps. The first one is the determination of states achieved beyond threshold. The next relates to the destabilisation of such states, and so on. The game is then repeated up to a point where the regime obtained is completely irregular. In this section we begin with a simple modelling of nonlinear effects in convection, §3.2.1. A brief account of experimental observations about the transition is then given in §3.2.2, where we point out the role of geometrical effects. This leads to a fundamental distinction between *confined* systems for which the concept of *temporal chaos* is relevant, §3.2.3, and *extended* systems for which the disorganisation in space is as important as the irregularity in time, i.e. *spatiotemporal chaos*, §3.2.4. We conclude the chapter with a brief presentation of convection in the post-transitional regime where the concept of *developed turbulence* begins to make sense, §3.2.5. Here we mostly stay at a phenomenological level, deferring the introduction of theoretical tools to subsequent chapters. A more in-depth presentation of experiments and related theory is to be found in [Getling (1998)].

### 3.2.1 Simplified model of nonlinear convection

Relation (3.22) defines a variable  $A$  measuring the intensity of the perturbation of the base state. At steady state, we thus expect  $A \equiv 0$  below threshold and  $A \neq 0$  above. In the theory of thermodynamic *phase transitions*  $A$  would be called an *order parameter* [Stanley (1988)]. However, (3.23) is valid only as long as  $A$  stays infinitesimal and must be completed to account for the range  $r > 0$ . In order to get (1.19), p. 13, we just postulated heuristically that convection was a self-limiting process and we

replaced  $\sigma$  in (3.23) by an effective value,<sup>3</sup>

$$\sigma_{\text{eff}} = \tau_0^{-1}(r - gA^2) \quad \text{with} \quad g > 0.$$

Beyond threshold, for  $r > 0$  ( $R > R_c$ ), several processes indeed come and limit the growth of  $A$ . First the dissipation increases, and second the destabilising force decreases since part of the heat is transported by the flow, so that the bulk effective temperature gradient that governs the conductive part of the heat flux decreases below its nominal value  $\beta$ .

It is of course possible to derive an accurate model of nonlinear evolution from the primitive equations in a systematic way. Here we rather continue to develop a heuristic formulation, guided by the result to be obtained. We no longer assume that  $P \gg 1$  but restrict ourselves to the consideration of the most unstable linear mode. On more general grounds than for (3.22), we then take  $\{v_z, \theta\} = \{V(t), \Theta(t)\} \sin(k_c x)$ , where  $V$  et  $\Theta$  are two time-dependent amplitudes. Injecting this assumption in (3.17, 3.18) we obtain:

$$\frac{d}{dt} V = P(\Theta - \pi^2 V), \quad (3.28)$$

$$\frac{d}{dt} \Theta = RV - \pi^2 \Theta. \quad (3.29)$$

System (3.28, 3.29) needs to be completed with nonlinear terms arising from the advection of the fluctuations  $\mathbf{v} \cdot \nabla \mathbf{v}$  and  $\mathbf{v} \cdot \nabla \theta$ . In the spirit of a first harmonic approximation now developed in space and not in time as for the van der Pol oscillator, p. 62, we guess that the terms that contribute are those resonating with the postulated dependence in  $\sin(k_c x)$ . From the continuity equation  $\partial_x v_x + \partial_z v_z = 0$ , assuming  $v_z \propto \sin(k_c x)$  one gets  $v_x \propto \cos(k_c x)$ , so that, in the equation for  $v_z$ , the advection term  $v_x \partial_x v_z + v_z \partial_z v_z$  varies as  $\sin^2(k_c x) = \frac{1}{2}(1 - \cos(2k_c x))$ , i.e. produces nothing in resonance with  $\sin(k_c x)$ . Averaging over the thickness of the layer and over a wavelength, we thus expect a negligible contribution from these terms to (3.28) which remains unchanged at this order.

The problem is different for (3.29). As a matter of fact, a parallel argument would also imply no complementary term, but this would not reflect the fact that, as indicated above, part of the heat is transported by the convection motion. The corresponding flux is easily identified with the product  $v_z \theta$ . As discussed in Sec. 3.1.2, below threshold, the destabilising part of the convection mechanism relies on the advection, due to differential buoyancy, of temperature fluctuations in a purely conductive temperature gradient. Above threshold, since part of the heat is transported

<sup>3</sup>Notation  $g$  introduced to measure the intensity of nonlinear couplings is traditional. In the context of convection it should not be mistaken with the gravitational acceleration, but the risk is limited.

by convection, differential buoyancy has to be appreciated with respect to a conductive temperature gradient  $\beta_{\text{eff}}$  which is decreased by the contribution of convection from its nominal value  $\beta$  evaluated from the applied temperature. That contribution,  $v_z\theta \propto \sin^2(k_c x)$ , produces: (i) a second harmonic component  $\propto \cos(2k_c x)$  that averages to zero over a fluctuation wavelength, but also (ii) a term at  $k = 0$  that corresponds to a correction brought to the averaged temperature profile.

Considering this correction as a variable in itself, let us call it  $\Psi$  and look for its governing equation. A simple calculation then yields:

$$\frac{d}{dt}\Psi = V\Theta - b\Psi, \quad (3.30)$$

where the first term on the right hand side is the source term issued from space-independent part of  $v_z\theta$  – contribution (ii) above – and the second term accounts for its diffusive relaxation according to the Fourier law, at a decay rate  $b$  that could be computed explicitly.

The argument about the effective intensity of the convection mechanism sketched above is simply implemented by subtracting the convective contribution  $\Psi$  from the nominal Rayleigh number  $R$  to form an effective Rayleigh number  $R_{\text{eff}}$  replacing it in (3.29). This yields:

$$\frac{d}{dt}\Theta = (R - \Psi)V - \pi^2\Theta. \quad (3.31)$$

Equations (3.28, 3.31, 3.30) generalise the linear model derived previously. They form the celebrated *Lorenz model* that played an important role in the development of ideas about chaos since 1963 (Note 6, p. 17), its original expression being recovered by appropriately re-scaling time, variables  $V$ ,  $\Theta$ ,  $\Psi$ , and parameter  $R$ . See §B.4.2, p. 420 for a hands-on study.

Let us first show how this model allows one to recover the effective Landau equation (1.19) introduced p. 13, extending (3.23) to the nonlinear regime. As noticed earlier, close to the threshold, the dynamics of the system is very slow. Its evolution rate is proportional to  $r = (R - R_c)/R_c \ll 1$ . But equation (3.30) shows that the natural relaxation time of correction  $\Psi$  remains  $\mathcal{O}(1)$ . We can thus assume that  $\Psi$  rapidly relaxes towards a value  $V\Theta/b$ , itself slowly varying at a rate  $\mathcal{O}(r)$ . Let us insert this value in (3.31) and admit that  $V = \Theta/\pi^2$  for all times, which, from (3.28), is true only in the limit  $P \rightarrow \infty$ . We get:

$$\frac{d}{dt}\Theta = [(R/\pi^2) - \pi^2]\Theta - \Theta^3/\pi^4 b,$$

which we rewrite as:

$$\frac{1}{\pi^2} \frac{d}{dt}\Theta = \frac{R - \pi^4}{\pi^4}\Theta - \frac{1}{b\pi^6}\Theta^3. \quad (3.32)$$

This equation is therefore exactly (1.19), i.e. :

$$\tau_0 \frac{d}{dt} A = rA - gA^3, \quad (3.33)$$

with  $\Theta$ , the amplitude of the temperature modulation playing the role of the effective variable  $A$ ,  $\tau_0 = 1/\pi^2$ ,  $r = (R - R_c)/R_c$ ,  $R_c = \pi^4$ , and  $g = 1/b\pi^6$ .

Obtaining the effective equation (3.33) is an example of reduction by *adiabatic elimination of enslaved variables*. Here variables  $V$  and  $\Psi$  are enslaved to  $\Theta$ : At every instant their values are fixed by that of  $\Theta \equiv A$  according to relations  $V = \Theta/\pi^2$  and  $\Psi = \Theta^2/b\pi^2$ . This step plays an essential role in the study of nonlinear dissipative systems.

Equation (3.33) accounts for the bifurcation from the conduction branch corresponding to the trivial solution  $A \equiv 0$  towards the convection branch associated to the pair of (here time-independent) nontrivial solutions. These *bifurcated solutions*,  $A_{(\pm)} = \pm\sqrt{r/g}$ , are given by the condition  $\frac{d}{dt}A = 0$ , and therefore correspond to *fixed points* of (3.33). Quantity  $g$  is positive, so that they exist for  $r > 0$ : the bifurcation is *supercritical*. All this has already been presented in the introductory chapter, see Figure 1.4 p. 13, and will be extended to general systems involving a single stationary mode in Chapter 4, especially in Exercise 4.4.4, p. 165.

We have previously stated without justification that the bifurcated solutions corresponding to convection beyond threshold are stable. Let us show how this arises from (3.33) using tools introduced in Chapter 2. Setting  $A = +\sqrt{r/g} + A'$ , we easily get the equation for perturbation  $A'$  by substitution. After simplification we obtain

$$\tau_0 \frac{d}{dt} A' = -2rA', \quad (3.34)$$

so that  $A'$  decays for  $r > 0$ . In fact this is valid only close enough to the threshold, before new instabilities have any chance to set in.

The argument developed above only holds as long as  $R \approx R_c$ . When  $R \gg R_c$ , the relaxation time of  $\Theta$  and  $V$  towards their equilibrium values, derived from (3.34), infinite at threshold, shortens as  $r$  increases and rapidly becomes of the order of magnitude of relaxation time of  $\Psi$ . Adiabatic elimination of the latter is then no longer legitimate:  $\Psi$  is less and less enslaved to  $\Theta$  and  $V$  but on the contrary gains a status of genuine degree of freedom.

### 3.2.2 Transition to turbulence of convection cells

Let us now consider nonlinear convection from an experimental point of view. The actual situation is less transparent than what has just been

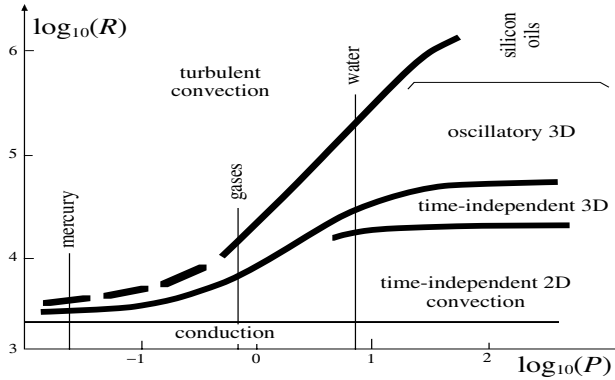


Fig. 3.4 Transition toward turbulence in convection, after Krishnamurti, Note 4. The Prandtl number is varied by changing the fluid. The transition lines are intentionally made thick to indicate orders of magnitude rather than precise thresholds.

described by using the simplified model, but one fact remains: the effective dimension of the problem increases with  $R$ . Unfortunately, the physical mechanisms that destabilise the cellular structure to produce the *secondary modes* are much less intuitive than the primary mechanism.

In principle, the method is the same as for the primary mode but, at steady state, the base flow beyond threshold is now made of finite-amplitude time-independent convection cells. The study is considerably more complicated than when we had to deal with the uniform conducting state since the new base flow is periodic along one horizontal direction. Accordingly, the operator obtained through linearisation now explicitly depends on space, which forbids the direct recourse to Fourier transforms to solve the problem. This will be re-examined theoretically later. For the moment, let us describe the cascade towards turbulence from a phenomenological point of view.

The convection threshold was independent of the Prandtl number  $P$ , whose value just played some role in the nature of the primary mode, thermal when  $P \gg 1$ , hydrodynamic when  $P \ll 1$ . This simple fact has profound consequences on the shape of the secondary modes and the subsequent bifurcation cascade towards turbulence. A compilation of early results adapted from Krishnamurti<sup>4</sup> is displayed in Fig. 3.4.

<sup>4</sup>R. Krishnamurti, "Some further studies on the transition to turbulent convection," J. Fluid Mech. **60** (1973) 285.

Upon increasing  $R$ , the fluid layer first experiences a transition from pure conduction (fluid uniformly at rest) to two-dimensional time independent convection (2D: fluctuations depend locally on two coordinates,  $z$  and one coordinate in the direction perpendicular to the local direction of the convection rolls). At sufficiently large Prandtl number a three-dimensional regime sets in (3D: fluctuations now depend on  $x, y, z$ ); at first time-independent, next periodic, and eventually turbulent. At small  $P$  the domain of ‘time-independent two-dimensional’ convection is very narrow and an irregular time dependence rapidly sets in, here called “turbulent convection”.<sup>5</sup>

### 3.2.2.1 Large-Prandtl-number fluids

When  $P \gg 1$  (e.g. , with highly viscous oils), the temperature field drives everything, inducing the vertical velocity component directly and the horizontal component indirectly *via* the continuity condition.

Secondary instabilities specific to this case remain localised within thermal boundary layers close to the horizontal plates. These boundary layers get thinner and thinner as the Rayleigh number is increased and, at some point, they become unstable against the plain Rayleigh mechanism. A stationary secondary instability called *bimodal* sets in, with rolls oriented at right angles with the primary rolls and located in the thermal boundary layers. Since the fluctuations are now modulated in the three directions of space, the regime is labelled “time-independent 3D” in Figure 3.4 on p. 101. Time dependence next manifests itself as a periodic break-down and reformation of thermal boundary layers first analysed by Howard. Strict periodicity is then lost and an irregular dynamics sets in.

### 3.2.2.2 Intermediate- and low-Prandtl-number fluids

At smaller  $P$ , the situation is more confused. Busse and his collaborators have identified a large number of possible secondary modes leading to a complicated picture in the  $(R, P, k)$  parameter space called the *Busse balloon*, owing to the global shape of the region where straight rolls are stable. When  $P \sim 1$  (water, gases) or smaller (liquid metals), the velocity field becomes dominant through specific contributions of the advection term  $\mathbf{v} \cdot \nabla \mathbf{v}$ . The unstable secondary modes appear close to the convection threshold and occupy the whole thickness of the layer. Cells enter a kind

<sup>5</sup>For a review of higher instability modes in convection, consult: F.H. Busse, “Transition to turbulence in Rayleigh–Bénard convection,” in [Swinney and Gollub (1985)].

of free-wheel regime where friction on the plates is dealt with inside thin viscous boundary layers. Time dependence enters very early in the form of ‘Busse oscillations’ that are sorts of waves propagating along the convection rolls due to an inertial call-back of roll axis undulations. Most often it turns out to be difficult to identify a range of Rayleigh numbers over which the periodic behaviour is strictly regular, and the flow is often considered turbulent right at the onset of oscillations.

### 3.2.2.3 Transition towards turbulence, conceptual problems

At least for  $P \gg 1$  there seems to be a small number of well defined steps on the way between the conduction regime and turbulence. This apparently supports the viewpoint advanced by Ruelle et Takens in 1971 (note 5, p. 16) according to whom the stochastic behaviour, a fundamental property of turbulence, generically appears at the end of a short cascade of three or four bifurcations. Previously, Landau (note 4, p. 16) explained his understanding of turbulence as the result of an indefinite superposition of modes, each with its own time-space scale, i.e. quasi-periodicity with an infinite number of incommensurate frequencies. These two interpretations were sketched in Figure 1.7, p. 17.

In fact, neither of the Ruelle–Takens or Landau pictures offer a satisfactory interpretation of experimental results reported above (Figure 3.4). All observations were made in containers that were very wide in order to check theories developed for a laterally unbounded system. The so-obtained convection *patterns* were rarely regularly organised but on the contrary were inhomogeneous with lots of defects, so that the transition thresholds were not defined as sharply as a bifurcation point. Moreover, a slow residual time dependence was often observed.

Having recognised that these interpretation problems were mostly due to spatial disorder, which in turn resulted from the presence of a large number of cells, and that lateral boundaries at large distances were ineffective in maintaining long range order in the patterns, experimentalists have tried to better control the situation by turning to systems with a small number of cells, hence lateral dimensions of containers of basically the same order of magnitude as their heights.

*Confinement effects* can be appreciated through *aspect ratios* defined as

$$\Gamma = \ell/h, \quad (3.35)$$

where  $\ell$  represents the typical lateral extension of the system, see Figure 3.5. We shall re-examine their physical role later in Chapter 4, §4.1.

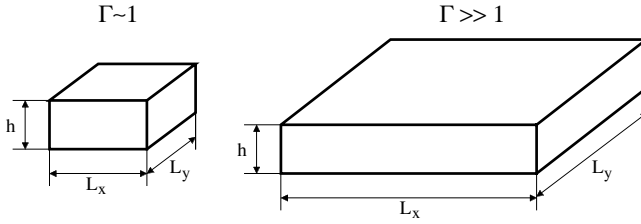


Fig. 3.5 Aspect ratio for closed systems, either confined (left) or extended (right).

Early experiments reported above were performed in the limit  $\Gamma \gg 1$  that characterise *extended systems* and for which the concept of *spatiotemporal chaos* to be introduced in Chapter 6 seems more appropriate. In contrast, strongly *confined* systems, characterised by  $\Gamma \sim 1$ , can be expected to better fit the framework proposed by Ruelle and Takens and their concept of *temporal chaos*. As a matter of fact, guaranteeing strong spatial coherence among a small number of convection cells, confinement effects should be instrumental in restricting the dynamics to couplings within a small set of effective variables.

### 3.2.3 Transition toward chaos in confined systems

The literature about the transition from regular to chaotic time behaviour is sufficiently rich that we can limit ourselves to the presentation of few experimental results obtained at the beginning of the eighties as typical examples of the main scenarios. This sketchy description is given mainly as an illustration of the kind of phenomena to be understood theoretically rather than as a review that would rather be premature at this stage. Consult the general bibliography for more detailed information, especially [Hao (1990); Cvitanović (1989)].

#### 3.2.3.1 Subharmonic cascade

The first experiment to be reported here has been performed by Libchaber et Maurer.<sup>6</sup> Liquid helium with  $P \sim 1$  is placed in a parallelepipedic container with aspect ratios  $\Gamma_x = 2.4$ ,  $\Gamma_y = 1.2$ . Stationary convection

<sup>6</sup>A. Libchaber and J. Maurer, "Une expérience de Rayleigh-Bénard en géométrie réduite; multiplication, accrochage et démultiplication de fréquences," *J. Physique Colloques* **41-C3** (1980) 51–56.

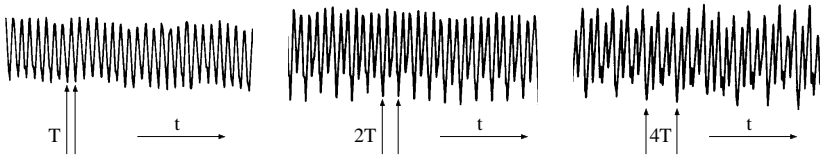


Fig. 3.6 Time series of the temperature signal measured at a given point during the first steps of a subharmonic cascade, after Libchaber and Maurer, Note 6.

sets in beyond some threshold  $R_c$ . At  $R \simeq 30R_c$  the system experiences a bifurcation toward an oscillatory regime. Then, at  $R \simeq 39.5R_c$ , a second mode with an incommensurate period sets in. This two-periodic regime persists up to  $R \simeq 40.5R_c$  when, while shifting, the second period gets locked to twice the first one, the system is then periodic with a period  $2T$ . The scenario under study now begins: a second period doubling (period  $4T$ ) at  $R \simeq 42.7R_c$  (Figure 3.6). After several supplementary period doublings (period  $8T$ ,  $16T$ , ... the system enters a chaotic regime for  $R > 43R_c$ . A complementary study of Fourier spectra would reveal first fine lines at one frequency and its harmonics, then a second family of lines and many combinations (two-periodic regime), then, after the locking, the return to a simpler spectrum with one fundamental line at  $\omega = 2\pi/T$  and its harmonics. The period doubling cascade manifests itself by the growth of *subharmonics* at  $\omega/2$ , next  $\omega/4$ , etc. As long as the system is periodic, no matter how long the period, the spectral lines remain narrow but when it becomes chaotic, they get measurably enlarged at their foot.

### 3.2.3.2 Chaos on a two-periodic background

This transition, closely reminiscent of the scenario originally proposed by Ruelle and Takens, has been observed roughly at the same epoch by Dubois and Bergé<sup>7</sup> again in parallelepipedic geometry with similar aspect ratios,  $\Gamma_x = 2$ ,  $\Gamma_y = 1.2$ , but this time with silicon oil ( $P \simeq 130$ ). In contrast with the previous experiment, visualisation of the structure was possible by means of differential interferometry, Figure 3.7, which made easier the understanding of motions at the origin of the observed fluctuations and the choice of points where to measure the velocity using a LASER Doppler anemometer.

The following sequence was observed: 1) conduction regime up to  $R_c$ .

<sup>7</sup>M. Dubois and P. Bergé, "Instabilités de couche limite dans un fluide en convection: évolution vers la turbulence," J. Physique **42** (1981) 167.

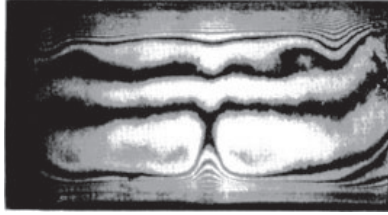


Fig. 3.7 Isotherms in silicon oil can be visualised by differential interferometry; the fringes originate from the variations of the refraction index induced by the local temperature gradients. (Courtesy M. Dubois.)

2) Time-independent convection from  $R_c$  to  $R \simeq 215R_c$ . 3) Bifurcation towards a periodic regime with period  $T_1$ . 4) Two-periodic dynamics with a second period  $T_2$  from  $R \simeq 250R_c$  up. Geographically well separated, the two oscillation modes are weakly coupled, which explains the relative robustness of the two-periodic regime and a characteristic alternation of locking/unlockings when the ratio of the periods, that slightly shifts with  $R$ , passes from incommensurate to commensurate values and *vice versa*. 5) For  $R > 305R_c$ , temporal chaos enters as an irregular slow modulation of a locked periodic behaviour that gives a series of widened spectral lines and low frequency power in the Fourier spectrum, Figure 3.8.

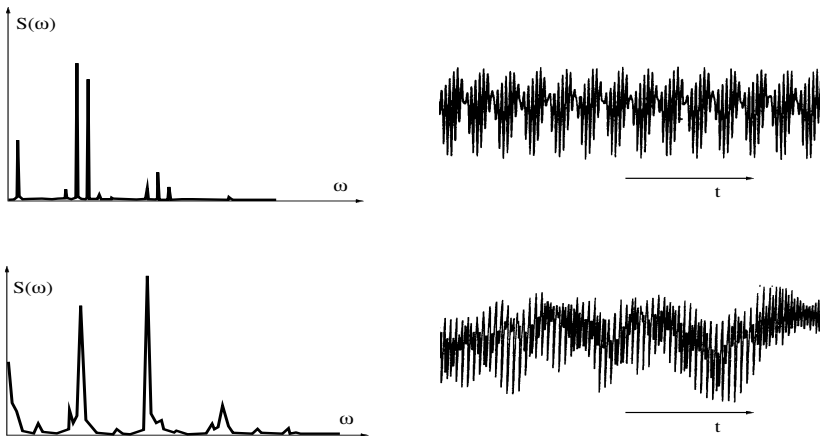


Fig. 3.8 Quasi-periodic convection in silicon oil. Fourier spectra (left) and time series (right) of a velocity component at a given point in the experimental cell. After Dubois and Bergé, Note 7.

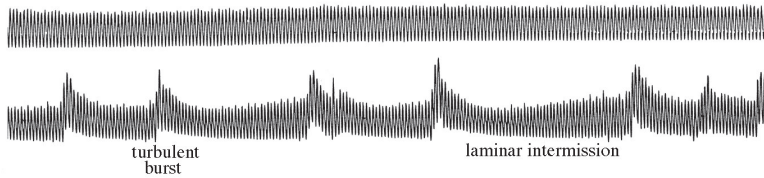


Fig. 3.9 The intermittency scenario: A periodic regime (“laminar” intermissions) is irregularly interrupted by chaotic bursts that become more frequent as  $R$  increases beyond the *intermittency threshold*. Upper trace: regular signal observed below threshold. Time is running from left to right. After Bergé *et al.*, Note 8.

### 3.2.3.3 Intermittency

The third scenario to be described here has also been observed by Bergé and Dubois<sup>8</sup> with the same fluid and the same experimental set-up but with a slightly different initial convection structure. Accordingly, a different transition scenario developed after a single step involving a secondary instability mechanism with a hot droplet transported by the general convection and playing the role of a pacemaker. Convection was time-independent up to  $R \simeq 250R_c$ , then periodic with period  $T$ . Not far above a subharmonic bifurcation (hence period  $2T$ ), for  $R = 290R_c$ , the system experienced a transition to chaos with irregularly distributed “turbulent” bursts interrupting the previously observed regular periodic behaviour forming “laminar” intermissions. When the Rayleigh number was increased, the frequency of the bursts was seen to increase. Time series of the velocity signal before and after the transition are displayed in Figure 3.9, upper trace and lower trace, respectively.

### 3.2.4 Dynamics of textures in extended systems

In contrast with what has just been described, before 1975 the transition to turbulence was studied in extended systems and focused more on the occurrence of a developed turbulent regime where most of the spatial structure was lost and the time dependence strongly irregular. The low frequency noise often observed at early stages was not recognised as an interesting phenomenon related to the transition process. The study of the emergence of chaos in confined systems has also led to reconsidering the situation for

<sup>8</sup>P. Bergé, M. Dubois, P. M., Y. Pomeau, “Intermittency in Rayleigh–Bénard convection,” *J. Physique Lettres* **41** (1980) L341–345.

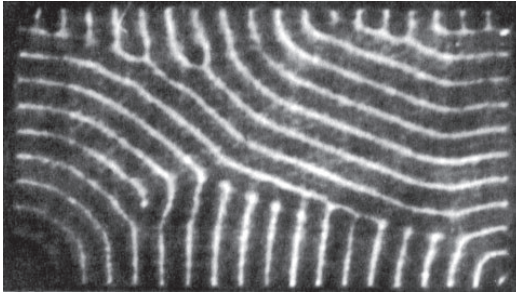


Fig. 3.10 Texture observed in convection at large Prandtl number as seen from above. (Courtesy V. Croquette.)

extended systems and introducing the notion of *spatiotemporal chaos* as an element of interpretation of the transition process. In practice, the instability mechanisms preserve coherence at the *local* scale (few convection cells) but are unable to maintain it on a *global* scale (the set-up). This can be understood as the result of the possible interference of a large number of neighbouring modes easily excited immediately beyond threshold (§3.1.5 and Chapter 6). Disordered patterns with many defects of all sorts, called *textures*, are generally observed in the absence of any induction process forcing the growth of regularly oriented “clean” convection structures. Here again we have to distinguish between fluids according to their Prandtl number.

#### 3.2.4.1 Textures in fluids with high Prandtl number

When  $P$  is large, quasi-stationary convection structures are obtained, which relates to the fact that the dominant field is the temperature, a scalar, and that the fluid layer mostly behaves as a gradient system (see §2.1.3, p. 47). It is then possible to interpret the principal features of the textures observed in terms of a single amplitude field. An example<sup>9</sup> is given in Figure 3.10, where one can easily identify *grains* of convection rolls with nearly uniform orientations, *grain boundaries* along which two grains with different orientations meet, *dislocations* where a pair of rolls suddenly ends. It should also be noted that rolls arrive mostly perpendicular to the lateral boundaries and that the frustration implied by this topological constraint is partly resolved by the presence of a large scale *curvature* of the rolls. The evolution of such textures is very slow, when compared to the velocity

<sup>9</sup>A. Pocheau and V. Croquette, “Dislocation motion: a wavenumber selection mechanism in Rayleigh–Bénard convection,” *J. Physique* **45** (1984) 35–48.

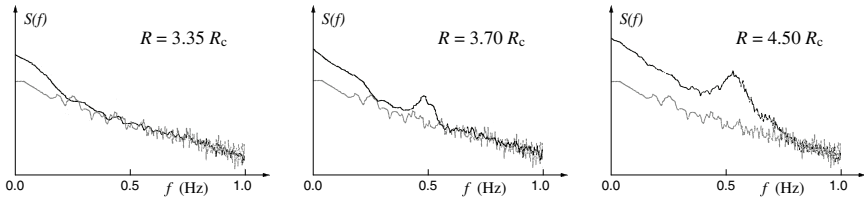


Fig. 3.11 Weak turbulence observed in a cylindrical cell with  $\Gamma = D/h = 12$  in liquid helium at low Prandtl number. Typical background noise is the grey line in each figure. For  $R = 3.35R_c$  low frequency noise develops first. At  $R = 3.70R_c$  noisy Busse oscillations at finite frequency around 0.5 Hz have settled in the system. As seen for  $R = 4.50R_c$  and beyond, the level of noise continues to increase gently. After Libchaber and Maurer, Note 10.

of the fluid. The transition from 2D to 3D convection mediated by defects, and the emergence of (weak) turbulence can be understood as a kind of melting of the global pattern, with progressive loss of local order.

#### 3.2.4.2 Transition at small Prandtl number and large aspect ratios

All experimental observations show that turbulence occurs early when  $P$  is small. This feature has to be attributed to the fact that the viscosity is low and that Reynolds numbers constructed from the velocity induced by convection and the size of the cells rapidly become large. Like for low-dimensional systems, the complexity of the dynamics is considerably enriched by inertial effects that favour oscillatory behaviour (here mainly Busse oscillations). This explains that mode interactions, even close to the convection threshold, generate a much more “active” behaviour than what is observed at higher Prandtl numbers. Another source of complexity comes from the existence of large scale flows directly generated by curvature and defects in the global texture.

Figure 3.11 illustrates the scenario observed again by Libchaber and Maurer<sup>10</sup> in liquid helium but in a cylindrical container with diameter  $D$  and aspect ratio  $\Gamma = D/h = 24$ . Remarkably enough, a low frequency noise sets in before any trace of secondary instability and when the latter develops (Busse oscillations) the system is already disordered so that the corresponding frequency is not sharply defined. It took some time before this behaviour could be understood.

<sup>10</sup>A. Libchaber and J. Maurer, “Local probe in a Rayleigh–Bénard experiment in liquid helium,” *J. Physique Lettres* **39** (1978) L369–L372.

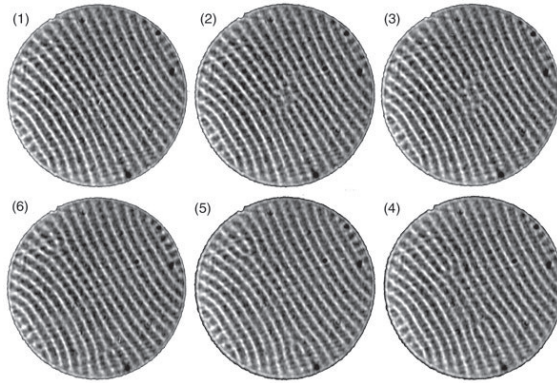


Fig. 3.12 Cyclic evolution from state (1)  $\rightarrow$  (2)  $\rightarrow$  ...  $\rightarrow$  (6)  $\rightarrow$  (1): Mechanism of nucleation–dissociation–migration–annihilation of dislocations pointed by Pocheau *et al.*, Note 11, and here illustrated with pictures kindly provided by V. Croquette from a similar experiment with  $\Gamma = D/h = 40$ .

In an experiment where helium was replaced by argon under pressure at room temperature, making visualisations possible, Pocheau *et al.*<sup>11</sup> later showed that the noise developing slightly above threshold was due to the synchronisation loss of an initially periodic process of nucleation, migration, annihilation of dislocations, as illustrated in Figure 3.12. The migration of dislocations was driven by a secondary flow at the scale of the container, the existence of which was predicted by earlier theoretical studies<sup>12</sup> and explicitly confirmed by specific experiments later.<sup>13</sup>

Again for low Prandtl numbers, somewhat above the range of Rayleigh numbers where the convection pattern is made of possibly slowly evolving, essentially straight rolls, a much more disorganised active state is observed in the form of rotating spirals as illustrated in Figure 3.13. This *spiral defect*

<sup>11</sup>A. Pocheau, V. Croquette, and P. Le Gal, “Turbulence in a cylindrical container of Argon near threshold of convection,” *Phys. Rev. Lett.* **55** (1985) 1094–1097, later reviewed by V. Croquette, “Convective Pattern Dynamics at Low Prandtl Number. Part I, II,” *Contemporary Physics* **30** (1989) 113–133, 153–171.

<sup>12</sup>(a) E.D. Siggia, A. Zippelius: “Pattern selection in Rayleigh–Bénard convection near threshold,” *Phys. Rev. Lett.* **47** (1981) 835–838. (b) P. Manneville, J.M. Piquemal: “Transverse phase diffusion in Rayleigh–Bénard convection,” *J. Physique Lettres* **43** (1982) L253–L258. (c) M.C. Cross, A.C. Newell: “Convection patterns in large aspect ratio systems,” *Physica D* **10** (1984) 299–328.

<sup>13</sup>V. Croquette *et al.* “Large-scale flow characterisation in a Rayleigh–Bénard convective pattern,” *Europhys. Lett.* **1** (1986) 393–399.

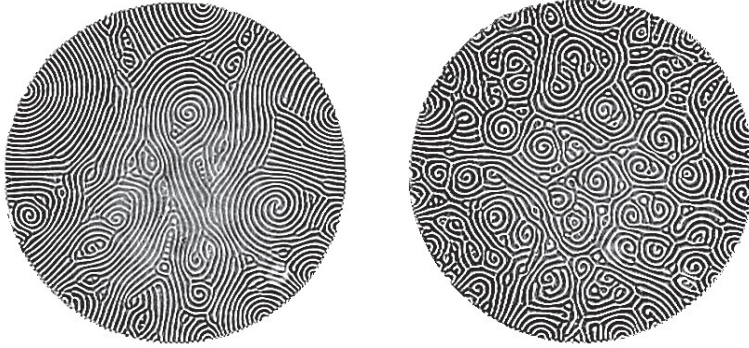


Fig. 3.13 Convection in  $\text{CO}_2$  with  $\Gamma = D/h \simeq 150$ , spiral defect chaos observed at  $r = 0.536$  (left) and  $r = 0.894$  (right). After Morris *et al.*, Note 14, courtesy G. Ahlers (UCSB).

*chaos*, observed in particular by Morris *et al.*<sup>14</sup> permanently evolves in both space and time. It takes place only at large aspect ratios but then does not depend on the lateral shape of the container. Furthermore, it is extensive in the sense that it can be characterised by a surface density of spiral cores seen to increase with increasing Rayleigh numbers beyond a threshold that depends on the Prandtl number. Curvature-induced secondary flows seem essential to its occurrence.

### 3.2.5 Turbulent convection

The local study of convection structures has been, since its very beginning, completed by measurements of the heat flux through the whole experimental container, characterising the global behaviour. Results are usually expressed in terms of the dimensionless *Nusselt number*:

$$N = \frac{\text{total heat flux}}{\text{conduction heat flux}}$$

where the total heat flux is the quantity actually measured and the conduction heat flux is the flux that would be computed from the temperature difference upon assuming that the fluid is at rest in the pure conduction state. Hence one gets  $N \equiv 1$  when  $R < R_c$ , while  $N - 1$  measures the

<sup>14</sup>S.W. Morris, E. Bodenschatz, D.S. Cannell, G. Ahlers, "The spatio-temporal structure of spiral-defect chaos," *Physica D* **97** (1996) 164–179.

contribution of convection. Close to threshold, one expects:

$$N - 1 \propto v_z \theta \propto \frac{R - R_c}{R_c}, \quad (3.36)$$

since both  $\theta$  and  $v_z$  vary as  $[(R - R_c)/R_c]^{1/2}$ , which is indeed well observed experimentally, see Figure 3.14, p. 113.

Far beyond threshold, from scaling arguments familiar in the theory of turbulence (Chapter 8), a power law behaviour is expected instead:

$$N \sim R^\gamma.$$

Early experiments seemed to support a theory by Malkus predicting  $\gamma = 1/3$  but the Rayleigh-number range studied was too narrow, while other studies for  $P \ll 1$  suggested rather  $\gamma = 1/4$ .

At the end of the eighties, the problem became a topic of renewed interest, experimental and theoretical. The heat flux was studied over  $R$ -ranges extending up to  $10^6$ , then  $10^{12}$  and even  $10^{17}$  in fluids with various Prandtl numbers and in containers with aspect ratio of order 1/2 or 1. Exponents  $\gamma$  ranging from 1/2 to 1/4, through 1/3, 0.3 or 2/7, have been measured over (sometimes very) limited ranges of Rayleigh numbers.<sup>15</sup>

In Figure 3.14 drawn after the results of Chavanne *et al.* in liquid helium, Note 15(c), one can identify the linear behaviour close to threshold expected from (3.36), a ‘soft turbulence’ regime where chaos is still mostly temporal as discussed in §3.2.3, then ‘hard turbulence’ with an exponent  $\gamma \simeq 2/7$  explained by a theory involving thermal transfer through turbulent layers sheared by the general circulation blowing as “wind” along the horizontal walls, and an “ultimate” regime with exponent tending to 1/2. The discussion bears on the existence of asymptotic regimes with a single exponent or rather on a superposition of power laws in the form  $N = C_1 R^{\gamma_1} + C_2 R^{\gamma_2}$  and the role of  $P$  (Note 15 d, e), of the geometry and nature of lateral walls, etc.

---

<sup>15</sup>We quote here only few references, first the general presentation by (a) E.D. Siggia, “High Rayleigh number convection,” *Annu. Rev. Fluid Mech.* **26** (1994) 137-168, and next specific results by (b) J.J. Niemela *et al.*, “Turbulent convection at very high Rayleigh numbers,” *Nature* **404** (2000) 837-840, err. **406** (2000) 439; (c) X. Chavanne *et al.*, “Turbulent Rayleigh-Bénard convection in gaseous and liquid He,” *Phys. Fluids* **13** (2001) 1300-1320; a theory by (d) S. Grossmann and D. Lohse, “Scaling in thermal convection: a unifying theory,” *J. Fluid Mech.* **407** (2000) 27-56 and “Thermal convection for large Prandtl numbers,” *Phys. Rev. Lett.* **86** (2001) 3316-3319; corresponding experimental work by (e) G. Ahlers and X.-c. Xu, “Prandtl-number dependence of heat transport in turbulent Rayleigh-Bénard convection,” *Phys. Rev. Lett.* **86** (2001) 3320-3323; (f) for a general review, consult: G. Ahlers et al: “Heat transfer and large scale dynamics in turbulent Rayleigh-Bénard convection,” *Rev. Mod. Phys.* **81** (2009) 503-537.

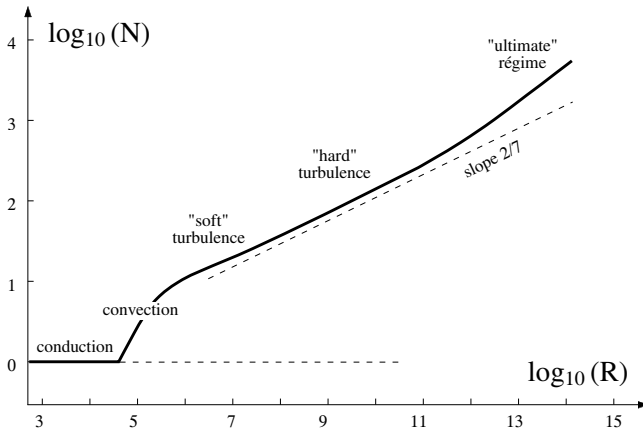


Fig. 3.14 Total heat flux as measured in terms of the Nusselt number as a function of the Rayleigh number (in log-log scale), after Chavanne *et al.*, Note 15(c).

To conclude, convection presents itself as the prototype of stationary cellular instabilities. In this chapter we have described its particularly intuitive mechanism, and its subsequent destabilisation up to turbulence. We have also noted the role of confinement effects on the nature of these steps. In the next three chapters we shall examine in more detail some mathematical aspects of the theory that allows us to interpret these phenomena and, at the same time, to tackle a large class of instabilities in continuous media. We shall not come back to turbulent convection, owing to the limited scope of Chapter 8 devoted to the simpler case of turbulent shear flows.

### 3.3 Exercises

#### 3.3.1 Simple model of cellular instability

Consider the linear part of the *Swift-Hohenberg model*<sup>16</sup> that reads:

$$\partial_t v = rv - (\nabla_{\perp}^2 + 1)^2 v. \quad (3.37)$$

This model accounts for the emergence of convection cells in a simplified but physically meaningful way and will be used further in §B.4.4–B.4.5.

Variable  $v$  may represent the vertical velocity component in the fluid or the departure from the base temperature profile,  $r$  is the control parameter

<sup>16</sup>J. Swift, P.C. Hohenberg: "Hydrodynamic fluctuations at the convective instability," *Phys. Rev. A* **15** (1977) 319–328.

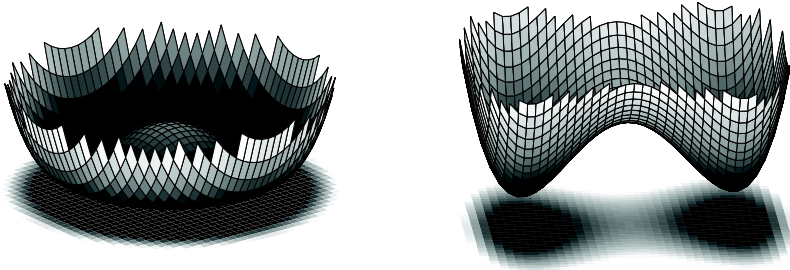


Fig. 3.15 Marginal stability surfaces for the linearised Swift-Hohenberg model in the isotropic (left) and anisotropic (right) cases.

measuring the relative distance to the threshold:  $r \propto (T - T_c)/T_c$ . In (3.37),  $\nabla_{\perp}^2 \equiv \partial_{xx} + \partial_{yy}$  is the Laplacian operator acting on the space dependence of the fluctuations in the plane of the layer.

1) Laterally unbounded medium.

a) Determine the dispersion relation  $s = s(\mathbf{k})$  for Fourier modes taken in the form  $\exp(i\mathbf{k} \cdot \mathbf{x})$  where  $\mathbf{k} = (k_x, k_y)$  and  $\mathbf{x} = (x, y)$ . Check that it depends only on  $k = |\mathbf{k}|$ .

b) Draw the graph of  $s(k)$  for  $r < 0$ ,  $r = 0$  and  $r > 0$  and conclude that the system bifurcates towards a cellular structure at  $r = 0$ . Show in particular that the most dangerous modes correspond to  $|\mathbf{k}| = 1$ .

c) Sketch the marginal stability surface ( $s(\mathbf{k}r) = 0$ ) in the three-dimensional space  $(k_x, k_y, r)$ ; determine the set of marginal modes and the domain of unstable wavevectors  $s(\mathbf{k}, r) > 0$  when  $r > 0$ . [Answer: Figure 3.15 (left).]

d) System (3.37) is isotropic in the  $(x-y)$  plane. Consider now the modified anisotropic model

$$\partial_t v = rv - [(\partial_{xx} + 1)^2 - \partial_{yy}] v. \quad (3.38)$$

Sketch the marginal stability surface for this case and conclude that, in contrast with the isotropic case, the linear stability operator selects a non degenerated mode. [Answer: Figure 3.15 (right).]

2) Consider now the same system but restricted to one space dimension:

$$\partial_t v = rv - (\partial_{xx} + 1)^2 v, \quad (3.39)$$

for a function  $v(x, t)$  defined on a finite interval of length  $\ell$  with boundary conditions  $v = \partial_{xx} v = 0$  at  $x = 0$  and  $x = \ell$ .

Check that the eigenmodes can be taken in the form  $V = A \sin(k_n x)$  with  $k_n = n\pi/\ell$ . Determine the marginal stability condition  $r = r_n^{(m)}(\ell)$  for mode  $n$  at given  $\ell$ , and next the instability threshold  $r_c(\ell) = \inf_n r_n^{(m)}(\ell)$ , as a function of  $\ell$ .

How does the spatial resonance between the intrinsic length-scale  $\lambda_c = 2\pi/k_c = 2\pi$  and the size  $\ell$  of the system manifest itself? Find the condition for two neighbouring modes being simultaneously marginal.

The reader is encouraged to perform the same (but much more difficult) study for boundary conditions  $v = \partial_x v = 0$  at  $x = \pm\ell/2$ . This is more typical of the general case since simple trigonometric lines are no longer appropriate. The eigenmodes will be searched for as a superposition of elementary solutions to the 4th order differential equation

$$sv = \left[ r - \left( \frac{d^2}{dx^2} + 1 \right)^2 \right] v$$

that fulfil the boundary conditions (the scalar  $s$  is the eigenvalue). Separate odd from even solutions and find corresponding marginal conditions (given by transcendental equations to be solved numerically by some root-finder program).

This model, completed by appropriate nonlinear terms, will be used again in Chapter 4, Exercise 4.4.2, and for the hands-on numerical experiments in §B.4.4–B.4.5.

### 3.3.2 Rayleigh–Bénard convection: detailed study

The purpose of the exercise is to go beyond the semi-quantitative approach developed in §3.1.4 and determine the marginal stability condition from the full primitive equations. The theory rests on the *Boussinesq approximation* of moderate heating which supports the idea that the fluid's physical parameters are independent of the temperature, except the density in the term responsible for the differential buoyancy force. The linearised thermo-hydrodynamic equations governing two-dimensional  $(x, z)$  perturbations then read<sup>17</sup>:

$$\partial_t(\partial_{xx} + \partial_{zz})v_z = P((\partial_{xx} + \partial_{zz})^2 v_z + \partial_{xx}\theta), \quad (3.40)$$

$$\partial_t\theta = Rv_z + (\partial_{xx} + \partial_{zz})\theta. \quad (3.41)$$

These equations are written here in dimensionless form after elimination of the pressure and horizontal velocity component. The scales are the same as

<sup>17</sup>These equations and the boundary conditions are derived below on p. 118.

those leading to (3.17, 3.18). As far as the  $(x, t)$ -dependence is considered, their structure is also the same as that of the simplified system, but they now retain the additional  $z$ -dependence of the fluctuations explicitly.

Boundary conditions are set at the position of the plates  $z_p$ , at top,  $z_t = 1$  or  $+1/2$ , and bottom  $z_b = 0$  or  $-1/2$ , one or the other choice making computations more transparent depending on the cases considered.

We consider here infinitely good heat-conducting horizontal plates. Accordingly the temperature is strictly fixed by heat baths so that the fluctuations are zero there:

$$\theta|_{z_p} = 0. \quad (3.42)$$

For the velocity components, rigid plates imply a *no-slip* condition

$$v_z|_{z_p} = \partial_z v_z|_{z_p} = 0. \quad (3.43)$$

In practice, calculations are easier with the somewhat artificial *stress-free* conditions considered initially by Rayleigh, which leads to the replacement of (3.43) by

$$v_z|_{z_p} = \partial_{zz} v_z|_{z_p} = 0. \quad (3.44)$$

In the following we consider symmetrical cases where top and bottom conditions are identical but any non-symmetrical condition (good/bad conductor, no-slip/stress-free) can be considered in the same way at the expense of a (much) more cumbersome analysis since parity considerations are no longer useful to classify the solutions.

1) Normal mode analysis in the stress-free case (Rayleigh solution, 1916). Boundary conditions are set at  $z_p = 0$  and 1.

a) For a laterally unbounded layer, check that solutions to (3.40, 3.41) can be taken in the form:

$$(v_z, \theta) = (\bar{V}, \bar{\Theta}) \sin(n\pi z) \exp(ikx) \exp(s_n t).$$

b) Determine the marginal stability condition for the mode  $n$  that first bifurcates when  $R$  is increased. Find the corresponding critical wavevector and threshold.

[Answer:

$$R_n^{(m)}(k) = (n^2\pi^2 + k^2)^3/k^2, \quad (3.45)$$

$k_c = \pi/\sqrt{2}$ ,  $R_c = 27\pi^4/4$ . See Figure 3.16, p. 118, curve A.]

c) Show that the linear dynamics close to the threshold is governed by:

$$\tau_0 s = r - \xi_0^2 (k - k_c)^2,$$

with  $r \equiv (R - R_c)/R_c$ . Compute coefficients  $\tau_0$  and  $\xi_0$ .

2) Normal mode analysis in the no-slip case. The exact solution, obtained by Pellew and Southwell (1940) is presented in [Chandrasekhar (1961)]. The corresponding marginal stability curve is given in Figure 3.16, p. 118, as line B' (fine, solid) with critical conditions  $k_c \approx 3.11632$ ,  $R_c \approx 1707.76$ .

Here we look for an approximate solution by a so-called *Galerkin method*, a special case of weighted-residual approximation introduced, e.g. in [Finlayson (1972)].

In a few words, the solution, expanded on a complete basis of functions, is further injected in the equations that are projected on a complementary basis using some scalar product. The Galerkin method comes in when the functions in the original and complementary bases are identical and fulfil the boundary conditions of the problem.

The approximate solution is seen to converge to the exact solution as the number of functions is increased, especially when the problem has an underlying variational structure, which is the case for Rayleigh–Bénard convection, as discussed in [Chandrasekhar (1961)].

Here, the solution of (3.40, 3.41) is searched for in the form:

$$\{v_z(x, z, t), \theta(x, z, t)\} = \{\bar{V}(z), \bar{\Theta}(z)\} \sin(k_x x) \exp(st).$$

The  $z$  dependence of  $\bar{V}_z$  and  $\bar{\Theta}$  is taken as polynomials. Boundary conditions are set at  $z = \pm 1/2$ .

a) Show that in order to fulfil boundary conditions automatically, one must take:

$$\begin{aligned} \bar{V}(z) &= \left(\frac{1}{4} - z^2\right)^2 P_v(z), \\ \bar{\Theta}(z) &= \left(\frac{1}{4} - z^2\right) P_\theta(z), \end{aligned}$$

where  $P_v(z)$  and  $P_\theta(z)$  are polynomials in  $z$ ,  $P_v(z) = \sum_{n=0}^{\infty} V_n z^n$ ,  $P_\theta(z) = \sum_{n=0}^{\infty} \Theta_n z^n$ . The approximation enters when polynomials are truncated beyond some given maximal degree  $N$ .

b) The differential problem being formally written as  $\mathcal{L}\mathbf{U} = 0$ , where  $\mathbf{U}$  has two components  $\bar{\Theta}$  et  $\bar{V}_z$ , the projection onto the basis is defined by integrals

$$\begin{aligned} \int_{1/2}^{1/2} z^n \left(\frac{1}{4} - z^2\right)^2 (\mathcal{L}\mathbf{U})_{v_z} dz &= 0, \\ \int_{1/2}^{1/2} z^n \left(\frac{1}{4} - z^2\right) (\mathcal{L}\mathbf{U})_{\theta} dz &= 0, \end{aligned}$$

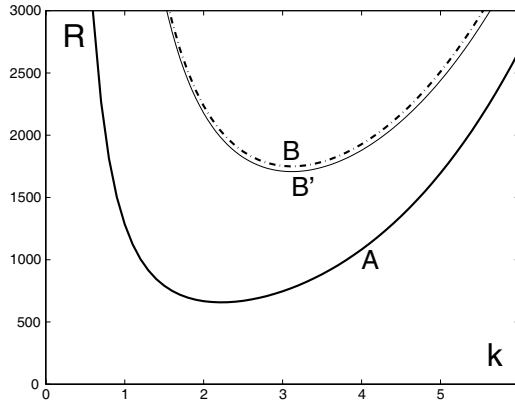


Fig. 3.16 Marginal stability curves of the most dangerous modes in the stress-free case (curve A) and no-slip case (curves B). Thin solid line  $\rightarrow$  exact result. Dot-dashed line  $\rightarrow$  Galerkin approximation at lowest significant order.

for  $n = 0, 1, \dots, N$ . This leads to a system of  $2(N + 1)$  linear equations for the  $2(N + 1)$  unknown coefficients introduced in the polynomials.

Considering only the stationary case at marginality, i.e.  $s = 0$ , derive the system at lowest significant order, i.e.  $N = 0$  (2 equations for 2 unknowns,  $\Theta_0$  and  $V_0$ ) and the corresponding marginal stability condition; compare the result to the Rayleigh solution (3.45). Then compute the critical wavevector and the threshold; further compare them to the exact result given above.

[Answer:

$$R^{(m)}(k) = \frac{28(k^4 + 24k^2 + 504)(k^2 + 10)}{27k^2}, \quad (3.46)$$

threshold:  $k_c \approx 3.1165 \simeq$  exact value,  $R_c \approx 1750$ , 2.5% too high only. See Figure 3.16, curve B (dot-dashed line), but so close an agreement is somehow accidental!]

*Derivation of system* (3.40–3.44).

In the two-dimensional case  $(x, z)$ , the continuity, Navier–Stokes and Fourier equations read:

$$\begin{aligned} \partial_x v_x + \partial_z v_z &= 0, \\ \rho(\partial_t v_x + v_x \partial_x v_x + v_z \partial_z v_x) &= -\partial_x p + \eta(\partial_{xx} + \partial_{zz})v_x, \\ \rho(\partial_t v_z + v_x \partial_x v_z + v_z \partial_z v_z) &= -\partial_z p + \eta(\partial_{xx} + \partial_{zz})v_z + g\alpha\theta, \\ \partial_t \theta + v_x \partial_x \theta + v_z \partial_z \theta &= \kappa(\partial_{xx} + \partial_{zz})\theta + \beta v_z. \end{aligned}$$

The formally quadratic terms have been dropped owing to the linearisation step. Following the usual procedure, pressure is eliminated by differentiating the equation for  $v_z$  with respect to  $x$ , the equation for  $v_x$  with respect to  $z$  and subtracting the two. In order to eliminate  $v_x$ , the result is further differentiated with respect to  $x$  and the so-obtained  $\partial_x v_x$  replaced with  $-\partial_z v_z$  using the continuity equation. This leads to:

$$\begin{aligned}\partial_t(\partial_{xx} + \partial_{zz})v_z &= \nu(\partial_{xx} + \partial_{zz})^2 v_z + \alpha g \partial_{xx} \theta, \\ \partial_t \theta &= \kappa(\partial_{xx} + \partial_{zz})\theta + \beta v_z,\end{aligned}$$

which is finally cast into (3.40, 3.41) by scaling  $v_z$  and  $\theta$  appropriately.

No-slip and stress-free boundary conditions respectively read  $v_x(z_p) = v_z(z_p) = 0$  and  $\partial_z v_x(z_p) = v_z(z_p) = 0$ . Differentiating the conditions on  $v_x$  with respect to  $x$  and replacing  $\partial_x v_x$  with  $-\partial_z v_z$  yields the boundary conditions (3.43, 3.44), expressed in terms of  $v_z$  exclusively.

### 3.3.3 Simplified model of convection in a binary mixture

Thermal convection in the presence of additional molecular diffusion processes is called *thermohaline*, by reference to the diffusion of salt in water. Here we consider the emergence of convection in a binary mixture. The local state of the fluid is thus characterised by the concentration  $C$  of a solute, in addition to its temperature  $T$  and its velocity  $\mathbf{v}$ . The temperature gradient is still generated by the temperature difference  $\Delta T$ , while a concentration gradient is applied by putting the fluid layer in contact with two reservoirs at different concentration through appropriate porous membranes. The solute concentration difference between top and bottom is a second control parameter and molecular diffusion (Fick law, coefficient  $D$ ) is a supplementary stabilising mechanism, while advection of the solute may contribute to the destabilisation of the layer. We develop a simplified one-dimensional model in the spirit of §3.1.2, i.e. assuming fluctuations that are functions of  $x$  and  $t$  only, while the driving gradients are imposed along the  $z$  direction.

1) Construction of the model:

The fluid layer is supposed to be at rest ( $\mathbf{v} \equiv 0$ ) in contact with two baths at temperatures  $T_t$  and  $T_b = T_t + \Delta T$  (heating from below implies  $\Delta T > 0$ ) and concentrations  $C_t$  and  $C_b = C_t + \Delta C$  ( $\Delta C$  positive or negative). The purely diffusive temperature and concentration profiles read:

$$T(z) = T_b - \beta z \quad \text{and} \quad C(z) = C_b - \beta' z,$$

where  $\beta = \Delta T/h$  et  $\beta' = \Delta C/h$  are the applied gradients. The differential buoyancy force is still induced by variations of the density  $\rho$  but it now has two origins, thermal expansion and composition change. Accordingly, the state equation can be taken as

$$\rho = \rho_b(1 - \alpha\theta - \alpha'c),$$

where  $\alpha (> 0)$  is the same coefficient as that introduced previously and where the sign of  $\alpha'$  depends on the composition of the mixture. Justify the equations governing the linearised model:

$$\begin{aligned}\partial_t v_z &= \nu \partial_{x^2} v_z + g(\alpha\theta + \alpha'c), \\ \partial_t \theta &= \kappa \partial_{x^2} \theta + \beta v_z, \\ \partial_t c &= D \partial_{x^2} c + \beta' v_z,\end{aligned}$$

and explain the origin of terms  $\beta v_z$  and  $\beta' v_z$  and discuss in simple terms the possible instability mechanisms involving each fluctuation.

Take  $h$  as length unit,  $\tau_\theta = h^2/\kappa$  as time unit, introduce the Lewis number  $L = D/\kappa$  in addition to the Prandtl number  $P = \kappa/\nu$ , define the control parameters

$$R = \frac{\alpha g \Delta T h^3}{\kappa \nu} \quad \text{et} \quad R' = \frac{\alpha' g \Delta C h^3}{D \nu}$$

(thermal and chemical Rayleigh numbers) and, finally, cast these equations in the form

$$\begin{aligned}\partial_t v_z &= P(\partial_{x^2} v_z + \theta + Lc), \\ \partial_t \theta &= \partial_{x^2} \theta + R v_z, \\ \partial_t c &= L \partial_{x^2} c + R' v_z.\end{aligned}$$

Interpret the Lewis number from a physical viewpoint; what can be its order of magnitude in a liquid, in a gas?

2) Normal mode analysis:

a) Introducing  $\{v_z, \theta, c\} = \{V, \Theta, C\} \cos(kx) \exp(st)$ , write down the algebraic linear system fulfilled by the amplitudes  $\{V, \Theta, C\}$ . (Here we assume directly and without justification that  $k \sim \pi$  (i.e. in dimensional units  $\lambda = 2h$  where  $\lambda$  is the wavelength of the unstable mode).

b) Show that for highly viscous fluids ( $P \rightarrow \infty$ ), the resulting system of three equations for three unknowns can be reduced to a system of two equations for two unknowns by eliminating the velocity component  $v_z$ . In the following we keep this supplementary assumption but the general case can

be treated in the same way using Exercise 2.5.3, p. 75.

c) Derive the compatibility condition of the simplified two-dimensional system and show that, in contrast with ordinary convection, complex roots are possible in the marginal case.

3) Different instability modes:

a) From a discussion of the sign of coefficients of the quadratic equation expressing the compatibility condition above, find the threshold of the stationary instability mode (the product of roots change its sign), then that of the oscillatory mode (the sum of roots change its sign).

b) In the parameter plane of parameters  $R'$  (horizontal axis) and  $R$ , draw the graph of these threshold conditions. Discuss the nature of the regime expected in each of the regions bound by these lines. Find the coordinates of the point where the system is simultaneously marginal against the two modes. Try to explain the physical origin of the oscillations by returning to the different contributions to the density changes and their respective relaxation times.

[Answer: Figure 3.17. The oscillations result from an interplay of differential buoyancy with two competing dissipation processes, one (thermal diffusion) being much faster than the other (molecular diffusion). This induces delays and phase shifts between the different fluctuations, ending in overshoots and oscillations.]

### 3.3.4 Turing patterns and reaction-diffusion systems.

In chemistry, mechanisms combining reaction and diffusion may produce dissipative structures called *Turing patterns*, as mentioned in §1.4.2, p. 27. Here we consider a simplified reaction–diffusion system where two species  $U$  and  $V$  with diffusion coefficients  $D_U$  and  $D_V$  also react with each other.

In one dimension, with coordinate  $x$ , the model reads:

$$\partial_t U = F_U(U, V) + D_U \partial_{xx} U, \quad (3.47)$$

$$\partial_t V = F_V(U, V) + D_V \partial_{xx} V, \quad (3.48)$$

where reaction terms  $F_U$  and  $F_V$  need not be specified at this stage.

1) Neglect diffusion ( $D_U = D_V \equiv 0$ ) and assume that a fixed point solution  $(U_0, V_0)$  exists; linearise the governing equations around that point, set

$$a = \partial_U F_U|_0, \quad b = \partial_V F_U|_0, \quad c = \partial_U F_V|_0, \quad d = \partial_V F_V|_0,$$

‘ $|_0$ ’ meaning computed at  $(U_0, V_0)$ , next determine the conditions on  $a, b, c, d$  that guarantee the stability of solution  $(U_0, V_0)$ .

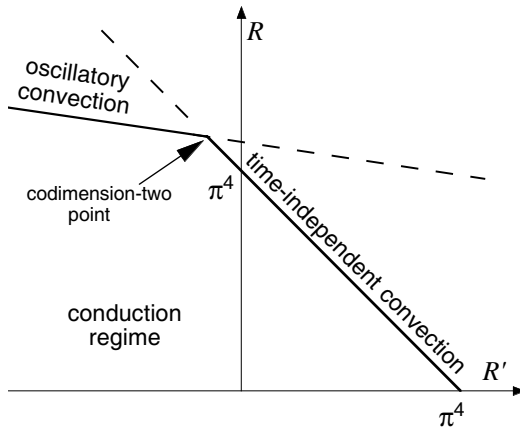


Fig. 3.17 Stability diagram for convection in a binary fluid mixture. When  $R' > 0$ , the temperature and concentration fluctuations co-operate, whereas when  $R' < 0$ , they play antagonistic roles. Oscillations occur as their evolutions get sufficiently out of phase. At the intersection of the two lines, called a *codimension-two* point (see p. 129) the two mechanisms are equally efficient to destabilise the layer.

[Answer: the linear stability matrix must have eigenvalues either real and negative or complex with negative real parts, hence negative sum ( $a+d < 0$ ) and positive product ( $ad - bc > 0$ ).]

2) Assume that these conditions are fulfilled and add the effect of diffusion ( $D_U \neq 0$ ,  $D_V \neq 0$ ). Determine the dispersion relation of fluctuations around the state  $(U_0, V_0)$  supposed uniform in space.

Write down the linearised system governing the amplitudes  $\bar{U}(t)$  and  $\bar{V}(t)$  of Fourier normal modes in  $\exp(ikx)$  and show that the instability, if any, is necessarily cellular and stationary ( $k \neq 0$ ,  $\omega = 0$ ).

Show that the occurrence of the instability requires:

$$aD_V + dD_U > 0 \quad \text{and} \quad 4(ad - bc)D_UD_V \leq (aD_V + dD_U)^2,$$

in addition to the conditions already found. When this is the case, determine the range of unstable wavevectors  $k$ .

### 3.3.5 Taylor–Couette instability

We study the stability of the flow between infinite coaxial cylinders rotating at different angular speeds (Couette flow). This problem was studied by Rayleigh (1916) at the limit of zero viscosity. Taylor (1923) developed the

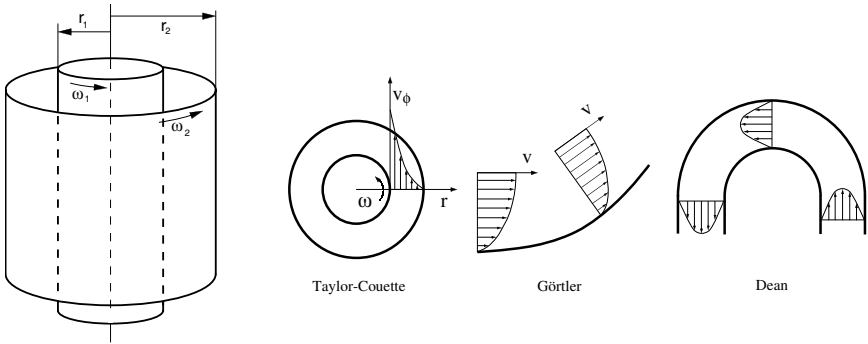


Fig. 3.18 Left: Geometry of the Taylor–Couette experiment. Right: Examples of curved flows.

first theoretical analysis of the viscous case and performed the corresponding experiments.

In the geometry of Figure 3.18 (left), assume that the base flow is purely azimuthal, show that  $v_\phi = r\omega_0(r)$  with

$$\omega_0(r) = a + b/r^2, \tag{3.49}$$

obtain  $a$  and  $b$  from the no-slip condition  $\omega(r_i) = \omega_i$  at  $r_i, i = 1, 2$ .

[Answer:  $a = (\omega_2 r_2^2 - \omega_1 r_1^2)/(r_2^2 - r_1^2), b = (\omega_1 - \omega_2)r_1^2 r_2^2/(r_2^2 - r_1^2)$ .]

1) Rayleigh instability mechanism (see also [Chandrasekhar (1961)] or [Drazin and Reid (1981)]). The base flow is characterised by the fact that the centrifugal force at distance  $r$  from the axis,  $\rho r \omega^2(r)$ , is compensated by a centripetal pressure gradient.

Consider a rotating fluid particle displaced from distance  $r$  to distance  $r + \delta r > r$ . In the absence of viscous friction, angular momentum  $\rho r v_\phi$  is a conserved quantity. From this conservation law, derive its angular speed at the new position and compare it with that of a fluid particle originally at the same place.

2) If the speed of the displaced particle is smaller than that of the surrounding fluid, the local pressure gradient is larger and pushes the particle back to its original position, the purely azimuthal flow is stable. In the opposite situation it is unstable. Show that this stability condition reads

$$\frac{d\omega}{dr} \delta r \geq -2 \frac{\omega}{r} \delta r,$$

then turn it to the form:

$$\delta (r^2 \omega) \geq 0$$

and express this *Rayleigh stability criterion* in words.

3) Application to the Couette profile and other curved flows.

a) Coming back to the base flow profile (3.49) identify the different possible cases (rotation direction identical or different, and when the rotation directions are identical, which cylinder is rotating faster) and find the situations that are stable according to the Rayleigh criterion.

b) When cylinders rotate in opposite directions, determine the region which is stable according to Rayleigh.

c) By comparison with the case of convection, and by anticipation of Chapter 7 about shear flows, guess the role of viscosity, especially when the flow is mechanically stable.

d) The same instability mechanism is expected to work when flow lines are curved. Identify the regions of the flow where the centrifugal instability can develop according to Rayleigh, in the boundary layer flow along a concave wall (Görtler instability; what about a convex wall?) or in the flow along a curved channel (Dean instability) depicted in Figure. 3.18 (right).